Non-Destructive Identification of GFRP Rebar Using Spatial Averaging of GPR Radargrams

YAEJIN PARK and HYUNG JIN LIM

ABSTRACT

This study presents the development of a non-destructive Glass Fiber Reinforced Polymer (GFRP) rebar identification technique for reinforced concrete structures based on Ground Penetrating Radar (GPR) B-scan images (radargrams). Conventional steel rebars are vulnerable to corrosion, and the consequential weakening of concrete from the inside can lead to the catastrophic failure of concrete structures. In addition, even when corrosion is detected, the damage is far advanced, leading to costly repairs and maintenance. Recently, GFRP rebars have been gaining interest because of their lightweight, non-corrosive, and high tensile strength characteristics, combating the limitations of conventional steel rebars. GPR is one of the non-destructive inspection techniques for concrete structures using electromagnetic waves. The existence, location, and diameter of steel rebars can be identified using the electromagnetic waves reflected from steel rebars owing to the significant differences in dielectric constants between concrete and steel rebars. However, for GFRP rebars, it becomes challenging because the dielectric constant difference between GFRP rebars and concrete is much less than that of steel rebars. Thus, in this study, the GPR-based GFRP rebar identification technique is developed by averaging multiple radargrams obtained from adjacent line scanning paths (spatial averaging). Concrete specimens were fabricated by inserting actual GFRP rebars with various diameters. Then, the existence and location of the GFRP rebars were estimated using GPR radargrams. The performance of the developed technique was evaluated qualitatively by calculating the standard deviation of the noise component. The results indicate that GFRP rebars are more clearly identified using the developed technique.

INTRODUCTION

In South Korea, the recent frequent heavy snowfall in winter has increased due to climate change, resulting in a greater distribution of deicing agents and a rise in coastal salt exposure caused by typhoons to concrete infrastructures. Consequently, chloride ingress into concrete infrastructure has intensified, accelerating the corrosion of embedded steel reinforcing bars. This corrosion process has contributed significantly to

Yaejin Park, Hyung Jin Lim, Kyonggi University, 154-42 Gwnaggyosan-Ro, Iui-dong, Yeongtong-Gu, Suwon, 16227, South Korea

structural defects and the premature deterioration of concrete infrastructures [1]. Moreover, manufacturing conventional steel rebars emits high amounts of carbon dioxide because coal is heavily used as a fuel source. Thus, the unit cost of steel rebars has increased to introduce new technologies and supplementary processes for carbon emission reduction [2].

In response, extensive research has been conducted since the 1980s to develop alternative reinforcing materials, particularly Fiber-Reinforced Polymers (FRPs) [3]. Among these, Glass Fiber-Reinforced Polymer (GFRP) rebars have emerged as a promising non-metallic substitute with advantages: (1) High strength-to-weight ratio, making them significantly lighter yet stronger in tension compared to steel rebars, (2) Superior resistance to corrosion, as they are immune to chloride-induced and chemical degradation, and (3) Environmental sustainability, owing to their relatively low carbon footprint during production. Although the unit cost of GFRP rebars was once higher than that of conventional steel rebars, the recent escalation in the price of conventional steel rebars, driven by carbon reduction measures, has made GFRP rebars increasingly cost-competitive.

Ground Penetrating Radar (GPR) is one of the non-destructive inspection techniques for concrete structures using electromagnetic waves. The existence, location, and diameter of steel rebars can be identified, and the corrosion of rebars can also be detected using the electromagnetic waves reflected from steel rebars, based on the significant differences in dielectric constants between concrete and steel rebars [4-6]. However, for GFRP rebars, it becomes challenging because the dielectric constant difference between GFRP rebars and concrete is much less than that of steel rebars.

This study presents the development of a GPR-based GFRP rebar identification technique by averaging multiple GPR B-scan (radargram) images obtained from adjacent line scanning paths. For the experimental validation, concrete specimens were fabricated by inserting actual GFRP rebars. Then, the existence and location of the GFRP rebars were estimated. The improvement of GFRP rebar visibility of the developed technique was evaluated quantitatively by calculating the standard deviation of the noise component.

THEORETICAL BACKGROUNDS

Ground Penetrating Radar (GPR)-based concrete inspection

GPR can identify the material properties and internal structure of the target structure by radiating electromagnetic waves and analyzing the changes in the speed and amplitude of the reflected electromagnetic waves from a boundary with different electrical properties (dielectric constant) [7].

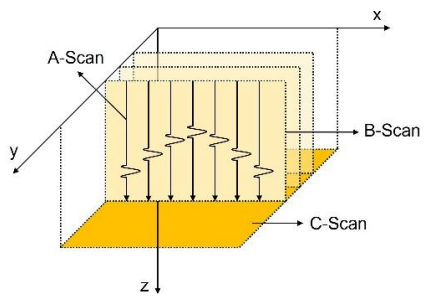

Figure 1. Representation of GPR scanning methods: A-scan, B-scan, C-scan

GPR inspection can be categorized into three scanning methods depending on the composition of the acquired signal (Fig. 1). First, A-scan acquires the amplitude of a single reflected wave, and the amplitude is expressed as time series data. Next, B-scan is a composition of two-dimensional amplitude data from multiple A-scans acquired at regular intervals along the line (line scanning). Finally, C-scan is a composition of three-dimensional amplitude data for an area constructed from multiple B-scans acquired at regular intervals across the region (area scanning) [8].

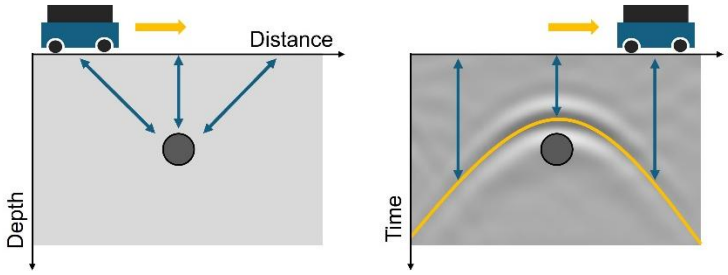

Figure 2. Ground penetrating radar (GPR) line scanning (B-Scan)

In particular, the line scanning (B-scan) is mainly used for GPR inspection, and the result of B-scan is called a radargram. As shown in Fig. 2, when a GPR moves on the surface of the target structure, A-scan data is obtained at regular intervals (blue arrows in left figure). At each data acquisition location, the distance from the surface and the buried object (e.g., rebars or voids) varies, which results in changes in both the amplitude and the arrival time of the reflected wave. As the acquired A-scan waveforms are arranged and visualized, a hyperbolic pattern (yellow curve in the right figure) can be obtained to identify the object [9].

Glass Fiber-Reinforced Polymer (GFRP) rebar detection

Physically, GPR can identify steel rebars using the significant differences in dielectric constants between concrete (5~10) and steel rebars (~300). However, for GFRP rebars, it becomes challenging because the dielectric constant difference between GFRP rebars and concrete is much less than that of steel rebars (4.5~5.5) [10-11]. As shown in Fig. 3, the radargram for steel rebar shows a clear hyperbolic pattern, while a blurry pattern is presented for GFRP rebar.

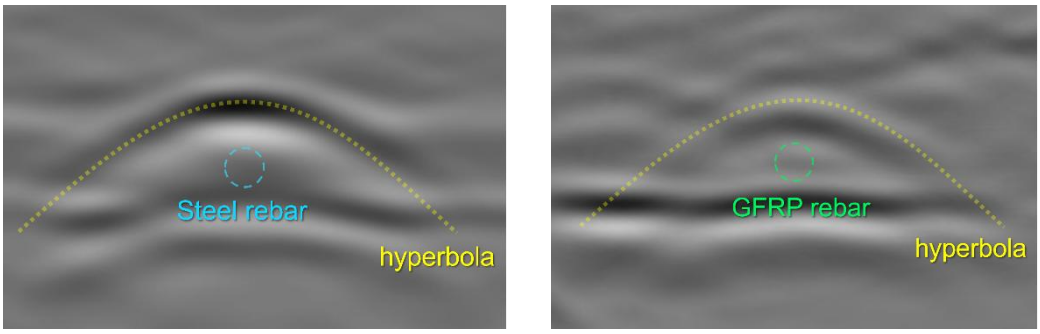

Steel rebar GFRP rebar

Figure 3. B-scan radargrams of steel and GFRP rebars

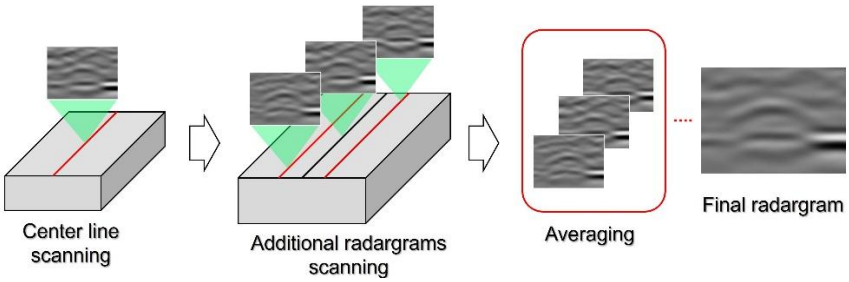

Figure 4. Schematics GFRP rebar detection technique using the spatial averaging

To tackle this problem, this study proposes the GPR-based GFRP rebar identification technique (Fig. 4). First, a radargram is obtained from a single line scanning on the target structure. Then, additional radargrams are obtained from multiple scanning paths adjacent to the initial scanning line. Finally, the final radargram for GFRP rebar identification is obtained by combining all radargrams (spatial averaging). During the averaging process, unexpected noise signals can be eliminated, and the weak electromagnetic waves reflected from GFRP rebar become vivid, because the location and diameter of GFRP rebar are identical to all radargrams.

EXPERIMENTAL VALIDATIONS

Specimen fabrication and data acquisition

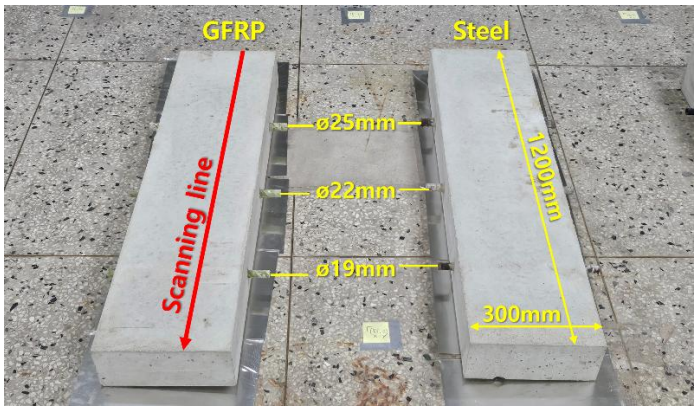

Figure 5. Specimen dimension and line scanning direction

Test specimens were fabricated by placing conventional steel and GFRP rebars with diameters of 25 mm, 22 mm, and 19 mm inside concrete, and the geometries of the specimens are shown in Figs. 5 and 6. Ordinary Portland Cement (OPC) with a specified compressive strength of 30 MPa and a water-cement ratio of 0.4 was used. The steel and GFRP rebars were placed at a depth of 70 mm from the surface. Here, actual GFRP rebars used for infrastructure construction, manufactured by DASAN Co., Ltd, were used.

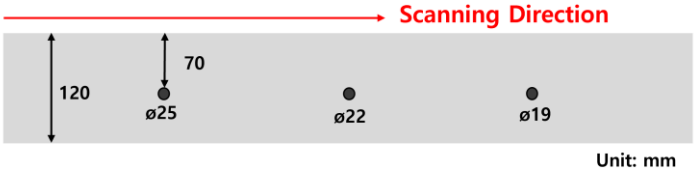

Figure 6. Rebar locations

Proceq GP8000 GPR was used as the data acquisition system. GP8000 generates electromagnetic waves with a frequency range of 200–4000 MHz for the inspection. The line scanning was performed perpendicular to the rebar as provided in Fig. 4. A total of 13-line scanning data (radargrams) were obtained at 10 mm intervals from the center line, as shown in Fig. 7. In addition, aluminum foils were placed under the specimens to intensify the reflected electromagnetic waves from the bottom of the specimens.

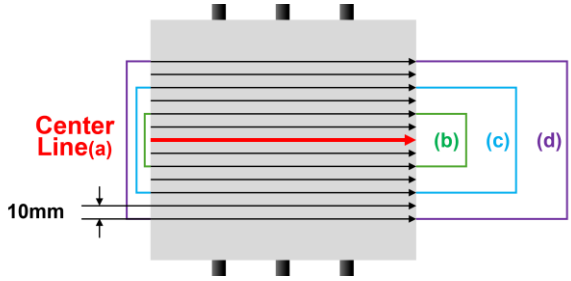

Figure 7. GPR line scanning for the spatial averaging (top view)

Experimental results

The performance of the proposed spatial averaging technique for GFRP rebar identification was evaluated by comparing the noise level with the number of radargrams used for the averaging. Here, the spatial averaging was performed by setting the opacity of each radargram to $1/n$, where n denotes the number of radargrams used for the averaging.

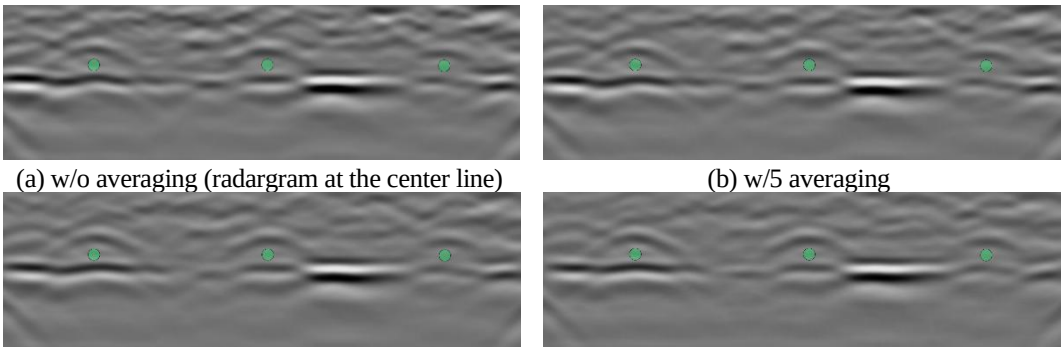

(a) w/o averaging (radargram at the center line) (b) w/5 averaging

(c) w/9 averaging (d) w/13 averaging

Figure 8. Effect of the number of radargrams on averaging (10 mm fixed interval)

To identify the optimal averaging scheme, various radargram combinations were tested. First, the effect of the number of radargrams for the averaging with a fixed scanning interval was investigated by averaging 1, 5, 9, and 13 radargrams with 10 mm intervals from the center line, as illustrated in Fig. 7 (a), (b), (c), and (d), respectively. The results are shown in Fig. 8, and the location of GFRP rebars is indicated by green circles. The results indicate that the GFRP radars become vivid as the number of radargrams for the averaging increases. For the quantitative evaluation, the standard deviation of the noise components is obtained without the GFRP rebar (Table I). A low standard deviation means that the pixel values are distributed closer to zero values, indicating a low noise level [12]. It was observed that as the number of radargrams included in the averaging increased, the standard deviation decreased correspondingly.

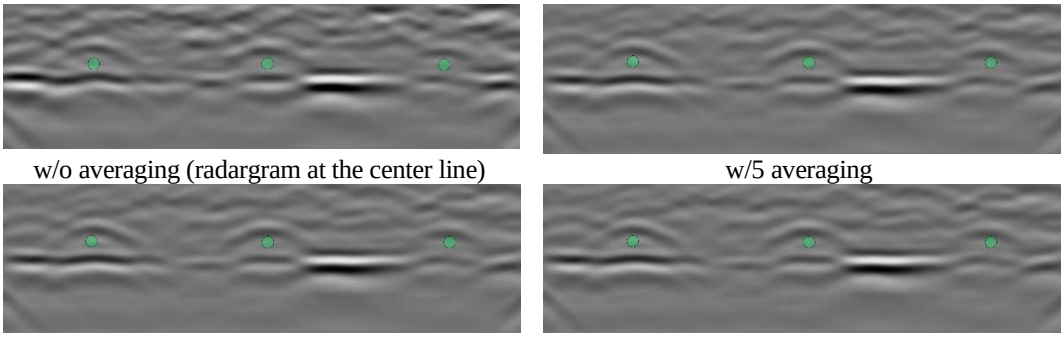

w/o averaging (radargram at the center line) w/5 averaging

w/7 averaging w/13 averaging

Figure 9. Effect of the number of radargrams on averaging (120 mm fixed range)

Second, the effect of the number of radargrams for the averaging within a fixed scanning range, averaging of 5 images at 30 mm intervals, 7 images at 20 mm intervals, and 13 images at 10 mm intervals within a 120 mm range (Fig. 9).

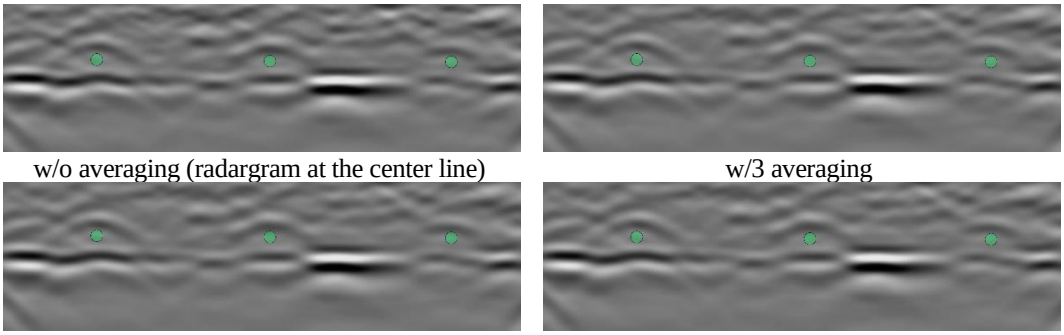

w/o averaging (radargram at the center line) w/3 averaging

w/5 averaging w/9 averaging

Figure 10. Effect of the number of radargrams on averaging (40 mm reduced range)

Table I. Standard deviation of the noise component of the averaged radargram

Method	**Interval (mm)**	**No. of Radargrams**	**Std. Dev.**
10 mm fixed interval (Fig.8)	-	1	6.105×10^{-2}
	10	5	5.715×10^{-2}
	10	9	5.234×10^{-2}
	10	13	5.006×10^{-2}
120 mm fixed range (Fig.9)	-	1	6.105×10^{-2}
	30	5	4.899×10^{-2}
	20	7	4.941×10^{-2}
	10	13	5.006×10^{-2}
40 mm reduced range (Fig.10)	-	1	6.105×10^{-2}
	20	3	5.893×10^{-2}
	10	5	5.819×10^{-2}
	5	9	5.819×10^{-2}

Third, reducing the scanning range, averaging of 3 images at 20 mm intervals, 5 images at 10 mm intervals, and 9 images at 5 mm intervals within a range of 40 mm were investigated (Fig. 10). The standard deviation of noise in each test is provided in Table I. The results show that better noise reduction performance can be obtained as the scanning range widens. Regarding the number of radargrams for the averaging, the noise level decreases as more radargrams are used. It is speculated that the background noise is sufficiently reduced by widening the range and increases again as more

radargrams are obtained from the closer interval. Additional studies with more diverse scanning intervals and ranges will be conducted to investigate this speculation.

CONCLUSIONS

This study proposes a GFRP rebar identification technique using the spatial averaging of multiple GPR radargrams. Concrete specimens were fabricated by inserting actual GFRP rebars for the experimental validation. The improvement of GFRP rebar visibility of the proposed technique was evaluated quantitatively by calculating the standard deviation of the noise component. Various spatial averaging schemes were tested, and the results show that the maximum noise reduction was obtained with the wide scanning range. Future works for 1) development of the post-processing of the averaged radargram to identify GFRP rebars diameter, 2) research on estimating the dielectric constant of concrete, and 3) further studies on the relationship between the scanning range and the interval for the optimal spatial averaging.

ACKNOWLEDGEMENT

This work was supported by the National Research Foundation of Korea (NRF) grant funded by the Korean government (Sejong Science Fellowship Program) (No. NRF-2021R1C1C2003318).

REFERENCES

1. Park, Y.-H., and Y. Choi. 2013. “Flexural Behaviors of GFRP Rebars Reinforced Concrete Beam under Accelerated Aging Environments,” Journal of the Korea Concrete Institute, 25(2):137–144.
2. Bhaskar, A., R. Abhishek, M. Assadi, and H. N. Somehesaraei. 2022. “Decarbonizing Primary Steel Production: Techno-Economic Assessment of a Hydrogen Based Green Steel Production Plant in Norway,” Journal of Cleaner Production, 350:131339.
3. American Concrete Institute. 2015. Guide for the Design and Construction of Structural Concrete Reinforced with Fiber-Reinforced Polymer (FRP) Bars, ACI 440.1R-15, American Concrete Institute.
4. Zanzi, L., and D. Arosio. 2013. “Sensitivity and Accuracy in Rebar Diameter Measurements from Dual-Polarized GPR Data,” Construction and Building Materials, 48:1293–1301.
5. Cheng, W., H.-H. Sun, K. H. Tan, and Z. Fan. 2023. “Estimating the Diameter of Reinforcing Bars Using an Ultra-Wideband MIMO GPR Array,” Construction and Building Materials, 365:129924.
6. Chang, C.-W., Tsai, C.-A., and Shiau, Y.-C. 2022. “Inspection of Steel Bars Corrosion in Reinforced Concrete Structures by Nondestructive Ground Penetrating Radar,” Applied Sciences, 12(11):5567.
7. Alsharahi, G., A. Faize, C. Maftei, M. Bayjja, M. Louzazni, A. Driouach, and A. Khamlichi. 2019. “Analysis and Modeling of GPR Signals to Detect Cavities: Case Studies in Morocco,” Journal of Electromagnetic Engineering and Science, 19(3):177–187.
8. Grasmueck, M., Weger, R., and Horstmeyer, H. (2005), Full resolution 3D GPR imaging. Geophysics, 70(1), K12-K19.
9. Zatar, W., Nghiem, H.-M., and Nguyen, H.-D. 2024. “Detecting Reinforced Concrete Rebars Using Ground Penetrating Radars,” Applied Sciences, 14(13):5808.
10. Ahmad, N. S., and R. Hamid. 2019. “Relationship between Moisture Content and Dielectric Values of Concrete using Ground Penetrating Radar Method,” Journal of Advanced Research Design, 57(1):21–33.
11. Naito, K., Kagawa, Y., Utsuno, S., Naganuma, T., and Kurihara, K. 2009. “Dielectric Properties of Woven Fabric Glass Fiber Reinforced Polymer-Matrix Composites in the THz Frequency Range,” Composites Science and Technology, 69(11–12):2027–2029.
12. Chen, G., Zhu, F., and Heng, P. A. 2015. “An Efficient Statistical Method for Image Noise Level Estimation,” in IEEE International Conference on Computer Vision (ICCV), pp. 477–485.